Synthesis of Highly Hydrophilic Cellulose and Graphene Oxide Based Membranes: Application in Alcohol Dehydration

Hasanvandi, Siavash; Mehdipour, Ebrahim*+, Shafieyoon, Parvaneh

Department of Chemistry, Faculty of Science, Lorestan University, Khorramabad, Lorestan, I.R. IRAN

ABSTRACT: *Combining highly ionic and very insoluble materials can be used to separate solvents with high water miscibility. In this work cellulose and Graphene Oxide (GO) were cross-linked by highly ionic N, N′-bis-(2-aminoethyl)-4,4′-dipyridinium bromide (BAEB) molecules to the preparation of CELL-BAEB and GO-BAEB membranes for alcohol dehydration. Fourier Transform InfraRed (FT-IR), proton nuclear magnetic resonance (^{1}HNMR), X-Ray Photoelectron Spectroscopy (XPS), Field Emission Scanning Electron Microscopy (FE-SEM), Energy Dispersive X-ray Spectroscopy (EDS), and Thermogravimetric Analysis (TGA) analyses were used to characterize the synthesized compounds. For ethanol, isopropyl alcohol (IPA), and n-butanol in a feed water concentration of 5-40 wt% and at a temperature range of 40-70°C, sorption parameters, including water content in the membrane, alcohol content in the membrane, swelling, and selectivity also pervaporation parameters, including water content in permeate, total flux, and separation factor, have been evaluated. The water content in the membrane was as high as 269 wt%, 276 wt%, 287 wt% for CELL-BAEB, and 188 wt%, 193 wt%, and 211 wt% for GO-BAEB in 40 wt% feed water at room temperature, and the separation factor was 3951, 4491, and 5616 for CELL-BAEB, and 2423, 3094, and 3741 for GO-BAEB in 10 wt% feed water at70 °C, for ethanol, IPA, and n-butanol, respectively. It was shown that the high flux and selective CELL-BAEB and GO-BAEB membranes are highly effective in separating water from alcohol.*

KEYWORDS: *Cellulose; Graphene oxide; Ionic cross-linker; Pervaporation; Alcohol dehydration.*

INTRODUCTION

Cellulose and GO are two compounds that are abundantly available in natural sources. The possibility of a wide variety of surface modifications and the abundance of natural resources will make these compounds more prominent in the future [1,2]. The modification of various materials in order to purify organic solvents, especially high-consuming alcohols, has been discussed in many articles [3-6]. A number of studies have been carried out to react GO with other molecules to obtain high performance membranes. Additionally, membranes made with pure GO showed a lot of special separation properties thanks to their 2D structure [7]. The unique structure and high charge density of viologen compounds have attracted much attention in recent years, and their use in molecular design continues to grow [8]. As a cross-linker, N,N′-bis-(2-aminoethyl)-4,4′-dipyridinium bromide (BAEB) was

* *To whom correspondence should be addressed.*
+ E-mail: e_mehdipour@yahoo.com & mehdipour.e@lu.ac.ir
1021-9986/2023/11/3799-3811 13/$/6.03

synthesized and used due to its high reaction tendency with aldehyde groups of dialdehyde cellulose (DAC) and epoxy groups of GO. Solvents such as ethanol, isopropyl alcohol (IPA), and n-butanol are important in industry and laboratories [9,10]. The use of ethanol as a replacement for fossil fuels is regarded as a potential green energy source in the coming years. The dehydration of ethanol is therefore crucial to obtaining high-purity ethanol for energy applications [11]. Propanol due to its miscibility, high flammability, and biocompatibility has a diverse range of application such as: use as solvent, fuel, electronic uses and medical uses [12]. For example, a large amount of IPA is used in the cleaning of semiconductors [13]. Butanol is also used in large quantities as a renewable biofuel [14]. The impurity of the water in these alcohols may cause adverse effects, so many attempts are made to dehydrate them. Convectional routes for the production of ethanol, IPA and n-butanol are through fermentation or chemical reaction [15,16]. However, there is usually some amount of water present in the produced alcohols. The common extraction process, such as distillation, suffers from low separation efficiencies, and other methods are required for purifying in industrial and laboratory scale [17]. A variety of mixtures can be separated by pervaporation, including miscible liquid mixtures, mixtures of isomers, and thermally unstable mixtures. In modern industry, pervaporation has been commercialized as a membrane-based separation technology that combines permeation and evaporation of liquid components across a membrane [18,19]. Pervaporation offers many advantages over conventional separation technologies, including energy efficiency, environmental friendliness, and high separation efficiency, particularly for the separation of azeotropic liquid mixtures [20,21]. For the dehydration of alcohols, two major types of membranes including: hydrophobic membranes [22] and hydrophilic membranes [23] are used. Due to the fact that water molecules cannot enter hydrophobic membranes, these membranes are not very efficient for separation in aqueous systems, and on the other hand, organic solvents cannot pass through membrane pores due to their larger molecular size [24]. Therefore, hydrophilic membranes can be used to separate organic solvents from water much more effectively [25]. A wide variety of hydrophilic membranes are used in the last decade such as: polyvinyl alcohol [26], organic-inorganic hybrids [27], polyimide [28], polyamides [29], and polyelectrolytes [30]. Hydrophilic groups are mostly responsible for the hydrophilicity of membranes. However, these groups may cause excessive swelling of the membrane, which eventually reduces its selectivity [31]. Viologen compounds have a high affinity for adsorbing water molecules, but they don't tend to dissolve even in short-chain alcohols due to their high ionic properties [32]. By using BAEB molecules as cross-linkers, a high level of selectivity and swelling can be achieved. A wide variety of chemical reactions are applied to prepare covalently cross-linked materials [33]. There have been a variety of research studies on alcohol dehydration membranes based on cross-linked polymers in recent years, such as Cross-linked poly(vinyl alcohol) with fumaric acid for pervaporation dehydration of 90/10 wt% IPA/water solution with separation factor of 550 and permeation flux of 1150 g/m^2.h at 60 ˚C [34], thermally cross-linked polyimide used for pervaporation dehydration of 85/15 wt% ethanol /water solution with separation factor of 670 and total flux of 110 g/m^2.h at 60˚C [35], cross-linked GO by sulfonated cyclodextrin for butanol pervaporation dehydration of 90/10 wt% n-butanol/water solution with separation factor of 1250 and permeation flux of 12490 g/m^2.h at 80˚C [36] and GO cross-linked by diamine monomers to for pervaporation dehydration of 90/10 wt% ethanol/water with separation factor of 1790 and total flux of 2297 g/m^2.h at 80ºC [37]. The reaction between amine and aldehyde groups of dialdehyde cellulose (DAC) and epoxy groups of GO is versatile due to the high reactivity of these functional groups [38]. Due to the high hydrophilicity of BAEB molecules, their grafting on the highly insoluble substrate of cellulose and GO, can be an innovative idea for producing a highly insoluble membrane with a strong tendency to separate water from high-consuming alcohols of ethanol, IPA, and n-butanol which are the key characteristics of efficient CELL-BAEB and GO-BAEB membranes. The highly hydrophilic synthesized membranes are very effective compared to other similar membranes in swelling and pervaporation parameters including: swelling, selectivity, water content in permeate, total flux, and separation factor.

EXPERIMENTAL SECTION

Materials

The following chemicals were used in the present study: N,N-dimethylformamide (DMF, Merck), potassium hydroxide (KOH, Merck), polyethersulfone (PES) was purchased from BASF (Ultrason-S6010, Germany),

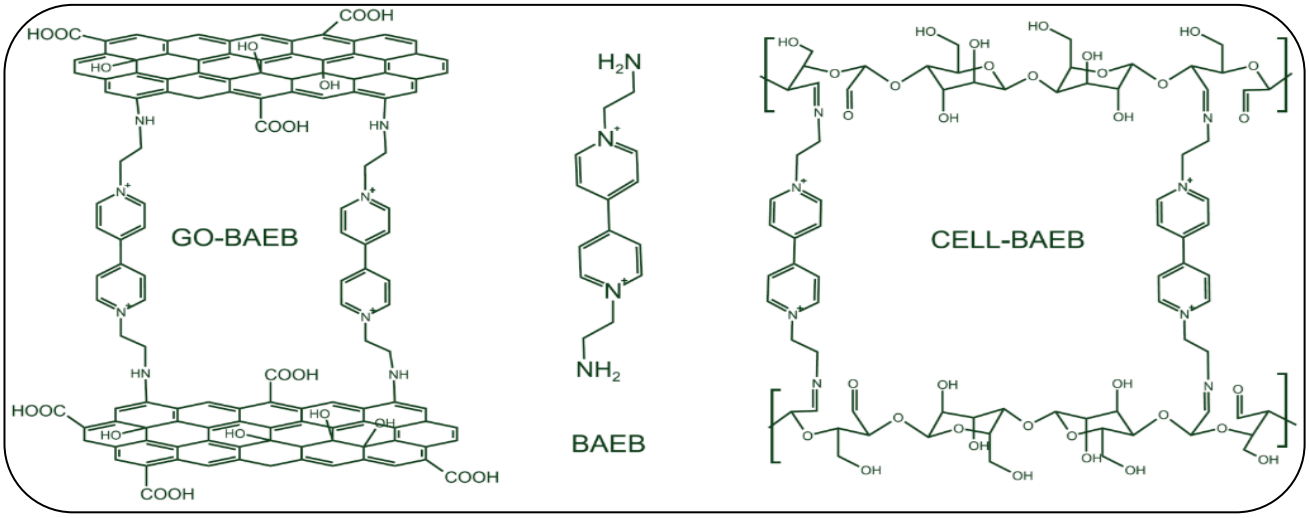

Scheme 1: Structure of BAEB, CELL-BAEB and GO-BAEB.

ethanol (>99%, Merck), 2-propanol (>99%, Merck), n-butanol (>99%, Merck), HCl (37%, Merck).

Characterizations

The morphology of the prepared materials was determined using a Field Emission Scanning Electron Microscope (FE-SEM, MIRA III, TESCAN, and the Czech Republic), and Energy Dispersive X-ray Spectroscopy (EDS) was carried out using SAMx EDS (France). The concentration of alcohol-H_2O in the solution was determined using a GC-14C gas chromatograph equipped with a flame ionization detector**.** Fourier-transform infrared (FT-IR) spectra were recorded on a SHIMADZU 8400 spectrophotometer using KBr pellets (4000-400 cm^{-1}). A powder X-Ray Diffractometer (XRD, Philips PW1730) equipped with a Cu X-ray tube (λ = 1.54 Å, 40 kV and 30 mA) was run at 0.05° sec^{-1} scan speed in the range of 2θ = 5 to 90°. X-ray Photoelectron Spectroscopy (XPS, Thermo Scientific, K-Alpha, USA) equipped with a monochromatic Al Kα radiation source was applied to study functional groups and the chemical composition of the compounds. ThermoGravimetric Analysis (TGA) was performed using a TGA (Q600 SDT, TA Instruments) with a heating rate of 10 °C/min at the temperature range from 40 °C to 900 °C in an N_2 atmosphere.

Synthesis procedures

Preparation of CELL-BAEB

BAEB (4.12 mmol), DAC (1 g), and 50 mL of distilled water were added to a 250 mL flask, and the pH was adjusted to 8 by adding NaOH (1 mol/L) to the solution. Then the mixture was heated in a water bath at 40°C for 8 h. Yellow-milky insoluble product was filtered and washed with distilled water, and then dried in a vacuum at 60°C for 4 h [39].

Preparation of GO-BAEB

The mixture of 0.25 g of GO, 0.90 g of BAEB, and 0.5 g of KOH was sonicated for 1 hour, then refluxed at 80 °C for 24 h. Synthesized GO-BAEB was centrifuged and washed with DI water, and then dried under a vacuum [40]. Scheme. 1 has shown BAEB, CELL-BAEB, and GO-BAEB structures.

Membranes preparation

Preparation of CELL-BAEB membrane

To prepare the CELL-BAEB membrane, a suspension of 2 wt% of CELL-BAEB in water at pH 7 was sonicated for 30 min. The resulting mixture was cast onto the PES filtration membrane (supplementary information). In order to remove residual solvent, the membrane was dried at 40 °C for 24 h, then dried again at 60 °C for 2 h.

Preparation of GO-BAEB membrane

For fabrication of the GO-BAEB membrane, GO-BAEB powder (1 mg/mL) was dispersed in water for 30 min using the ultrasonic device. GO-BAEB suspensions were filtered using a PES filter and then dried at 60 °C overnight to remove any remaining.

Swelling and sorption experiments

GO-BAEB and CELL-BAEB solutions were cast on a smooth glass substrate and dried under reduced pressure at 50°C to measure membrane swelling [41].

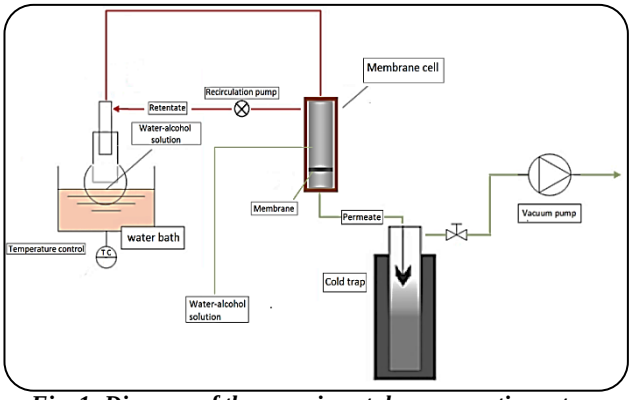

Fig. 1: Diagram of the experimental pervaporation setup.

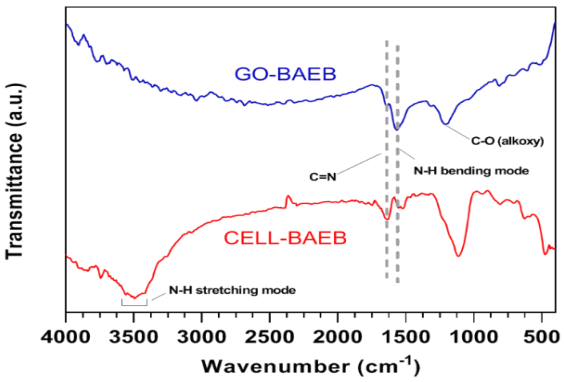

Fig. 2: FT-IR spectrum of CELL-BAEB and GO-BAEB.

GO-BAEB and CELL-BAEB were weighed and immersed in ethanol, IPA, and n-butanol solutions at various concentrations and allowed to reach sorption equilibrium at 30°C in a sealed glass flask. After a few minutes, the excess solvent on the membrane surface was quickly removed with filter paper and the degree of swelling was determined by the following equation:

$$DS = \frac{Ws - Wd}{Wd} \times 100 \quad (1)$$

The W_s and W_d indicate the weights of swollen and dried membranes, respectively. Water and alcohol concentrations in membranes can be determined by separating the sorbed solution. For this purpose, the swollen membrane was immersed in liquid nitrogen under reduced pressure and the collected solution was analyzed using a GC. The selectivity of membrane sorption (sor) is calculated as follows:

$$\alpha sor = \frac{MH2O/Malcohol}{FH2O/Falcohol} \quad (2)$$

M_{H2O}, $M_{alcohol}$, and F_{H2O}, $F_{alcohol}$ represent the weight fraction of water and alcohol in membrane and feed, respectively [42].

Pervaporation experiments

Fig. 1 shows the diagram of the homemade apparatus used to measure the pervaporation performance of membranes.

The feed temperature was maintained at 70 °C with continuous stirring. Using a centrifugal pump, the feed was circulated over the membrane with a flow rate of 220 l/h and a pressure of 1 bar. The permeate was collected every 20 min through suction by a vacuum pump (with a vacuum level below 300 Pa) in a glass cold trap within a Dewar flask containing liquid nitrogen. The active area of the used membrane was 10.2 cm^2. An electronic balance with an accuracy of 10^{-4} g was used to measure the total volume of permeate [43]. Under the same operating conditions, the measurements were repeated three times. The following equations were used to calculate the permeation flux (J) and membrane separation coefficient:

$$J = \frac{W}{At} \quad (3)$$

$$\alpha sep = \frac{PH2O/Pethanol}{FH2O/Fethanol} \quad (4)$$

Where $A(cm^2)$ is the effective membrane area, W(g) is the permeation weight at the operation time t; P_{H2O}, $P_{ethanol}$, and F_{H2O}, $F_{ethanol}$ represent the weight fractions of water and alcohol in the permeate and the feed, respectively.

RESULTS AND DISCUSSION

Characterizations of synthesized compounds

IR Spectroscopy

The FT-IR spectra of GO-BAEB and CELL-BAEB are shown in Fig. 2. The epoxy band in GO (Fig. S1b) has disappeared and a new absorption peak has been observed in GO-BAEB at 1554 cm^{-1}, associated with bending vibrations of N-H, resulted from nucleophilic substitution reaction of the epoxide group with the amine group [44]. The band at 1641 cm^{-1} is assigned to ν(C=N). New peaks confirmed the successful bonding of the amine-terminal of BAEB (Fig. S1b) to GO nanosheets. Compared to DAC (Fig. S1b), the peak at 1741 cm^{-1} of C=O stretching vibration has disappeared in the spectrum of CELL-BAEB. The strong absorption peak at 1640 cm-1 and the missing absorption band at 1741 cm^{-1} confirm the reaction of the aldehyde group of DAC with the amino groups of BAEB and the formation of Schiff base.

XPS analysis

A further investigation of GO and BAEB reactions was carried out with X-ray Photoelectron Spectroscopy (XPS).

Table 1: The elemental composition of GO and GO-BAEB analyzed by XPS.

sample	C (at. %)	N (at. %)	O (at. %)	C/O	C/N
GO	57.53	-	42.46	1.35	-
GO-BAEB	75.97	6.68	17.34	4.38	11.37

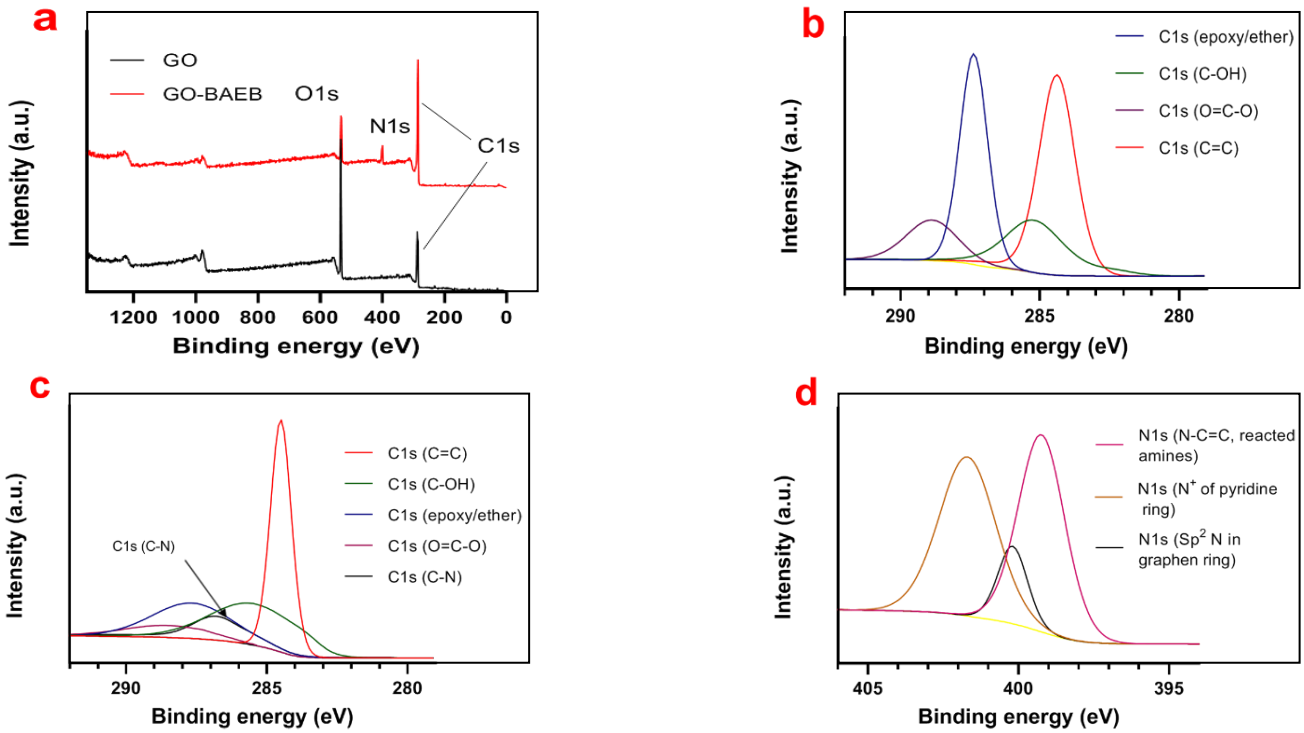

Fig. 3: The XPS survey curves of GO and GO-BAEB (a), inset: the higher resolution curves of the C1s region of GO (b) and C1s region of GO-BEAB (c) and N1s region of GO−BEAB (d).

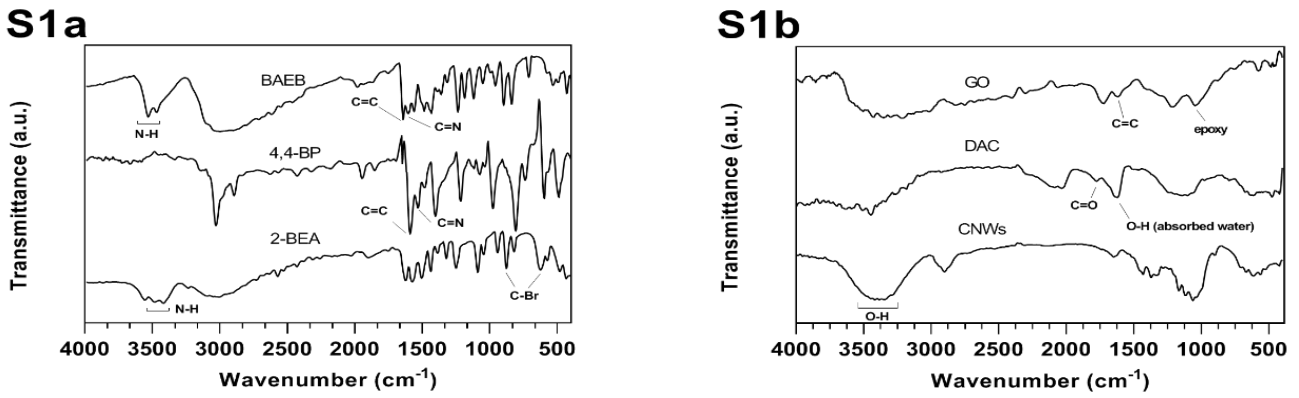

Fig. S1: a) FT-IR spectra of 2-BEA, 4,4-BP, and BAEB, S1b) FT-IR spectra of GO, CNWs and DAC.

Fig. 3. Shows the survey spectrum of the cross-linked compound as well as the higher-resolution spectra of the C1s and N1s areas. For GO and GO-BAEB, the survey spectra (Fig. 3a) yielded C/O atomic ratios of 1.35 and 4.38 (Table 1). In GO (Fig. 3b), four distinct peaks are clearly identifiable as carbon atoms located in different functional groups, including carbon in the GO sheet (284.28 eV), carbon in C-OH (285.38 eV), carbon in epoxy/ether groups (287.48 eV) and carbon in carbonyl groups (288.87 eV) [45]. XPS GO-BAEB spectrum (Fig. 3c) also confirms the oxygen

Table 2: Elemental composition of DAC and CELL-BAEB analyzed by EDS.

Sample	C (at. %)	N (at. %)	O (at. %)	C/O	C/N
DAC	53	-	47	1.13	-
CELL-BAEB	61.5	7.22	31.27	1.97	8.52

Fig. 4: FE-SEM images of a) GO, b) GO-BAEB, c) unmodified CNW, d) DAC and e) CELL-BAEB.

functional groups; there was a clear decrease in C amount in epoxy/ether groups. A new component corresponding to the C bond to N was observed at 286.68 eV while epoxy groups decreased significantly, indicating that BAEB and GO are covalently interacting. Four peaks can be fitted to the N 1s core-level spectrum of GO-BAEB (Fig. 3d). A peak at 401.69 eV can be assigned to the positively charged nitrogen (N+) in BAEB, a peak at 399.23 eV is related to an amine group (-N-C=) from BAEB and GO reactions, and a radical cation (N•+) probably formed during X-ray excitation [46], the peak at 400.19 eV with low intensity can be explained by the nitrogen (N) introduced into the graphene ring during the reaction with BAEB [47]. Contrary to GO, the GO-BAEB spectrum exhibits N1s peak, showing that BAEB is covalently functionalized by GO (Fig. 3a). In Table 1, N content for GO-BAEB is 6.68 atomic% [48].

SEM and EDS studies

The morphology of GO, GO-BAEB, CNWs, DAC, and CELL-BAEB was investigated by FE-SEM. The FE-SEM image of the GO shows a large number of nanosheets (Fig. 4a). The FE-SEM images of GO-BAEB (Fig. 4b) show that the sample consists of stacked nanosheets that appear to be formed by cross-linking GO sheets to BAEB molecules [48]. After oxidation and reaction with BAEB, the short rod-like structures of CNWs (Fig. 4c) exhibit a relatively dense structure, which may be the result of cross-linking between cellulose chains. A morphological difference was observed between the CELL-BAEB (Fig. 4e) and the DAC (Fig. 4d) [49]. When DAC reacts with BAEB, the bead shape of DAC disappears and CELL-BAEB exhibits a relatively dense surface structure, which may have been caused by cross-linking of the DAC [50]. EDS results in Table 2 indicate an increase in the C/N ratio and a decrease in the C/O ratio.

XRD studies

GO showed an intense peak at 2θ = 12.4°, showing an interlayer distance of 0.71 nm (Fig. S2a) [51]. GO-BAEB exhibits a peak at 2θ = 8.8°, which corresponds to the interlayer distance of 1.01 nm [52]. In GO-BAEB, the diffraction peak shifts to a lower angle, and the interlayer spacing increases as a result of intercalation (Fig. S2a) [37]. CNWs exhibited a strong peak at 22.7°, indicating high crystallinity; however, after oxidation, this peak became broad (Fig. S2b) [53]. There was a broad diffraction peak (17°-27°) in the XRD pattern of CELL-BAEB (Fig. S2b). CELL-BAEB has a relatively low crystallinity compared to DAC, indicating that Schiff base formation between DAC and BAEB can reduce the crystallinity of DAC [54].

TG analysis of GO, GO-BAEB, DAC, and CELL-BAEB

TGA analysis was performed to determine the weight losses of GO, GO-BAEB, DAC, and CELL-BAEB with temperature (Fig. 5). When GO is heated to 144 °C, it loses approximately 17% of its weight, which indicates evaporation of adsorbed and bounded water. At 200 °C, however, GO loses 37% of its mass due to the decomposition of oxygen-containing groups on its surface; hydroxyls, epoxy groups, and carboxyl groups [55]. Further, GO-BAEB showed a mass loss of 10% between 40°C and 137°C as well as a gradual mass loss of 26% between 245°C and 342°C, possibly due to the removal of

Fig. 5: a) TGA curves of GO, GO-BAEB and b) DAC and CELL-BAEB.

Fig. S2a) XRD patterns of GO, GO-BAEB and S2b) CNWs, DAC, and CELL- BAEB

BAEB molecules. Compared to the GO, the GO-BAEB appears to be more thermally stable, likely due to the reduction of oxygen-containing groups of the GO during reaction with diamine molecules [56]. In Fig. 5b, a small weight loss for both DAC (9%) and CELL-BAEB (17%) samples are observed below 100°C, which is due to the removal of absorbed water [57]. The DAC initiates decomposition around 355 °C while for CELL-BAEB, the more obvious decomposition occurs at 320°C. CELL-BAEB was less thermally stable than un-grafted DAC beads, which is related to the disruption of hydrogen bonds in unmodified DAC due to the reaction of the aldehyde groups with BAEB molecules [58]. Compared to DAC, the CELL-BAEB initiated thermal decomposition at a lower temperature, indicating that the grafting of BAEB on the DAC decreased its thermal stability.

Sorption and pervaporation measurements

Before using a membrane, it is important to evaluate its performance. The total flux, separation factor, swelling degree, and adsorption selectivity are some criteria used to evaluate membrane performance.

Sorption of alcohol-water mixtures

Sorption behavior study is one of the most important factors in evaluating a compound's efficiency in separating miscible solvents. The swelling of CELL-BAEB and GO-BAEB membranes as a function of water content is shown in Fig. 6c and Fig. 6f. As can be seen, swelling and water sorption increase with the increase of water content in the alcohol-water mixture. Moreover, the CELL-BAEB membrane has a higher swelling and water adsorption capacity. Ethanol sorption is different from other alcohols even when the ethanol content in the liquid decreases, the alcohol content in CELL-BAEB and GO-BAEB membranes continues to increase (Fig. 6b and Fig. 6e). It may be due to the high swelling degree of CELL-BAEB and GO-BAEB membranes as a result of their high hydrophilicity [59]. Fig. 6c and Fig. 6f, also show the sorption selectivity of CELL-BAEB and GO-BAEB membranes as a function of water content. There is a higher sorption selectivity for both membranes even at lower water contents. Additionally, CELL-BAEB membranes exhibit a greater decrease in sorption selectivity with increasing water content than GO-BAEB membranes,

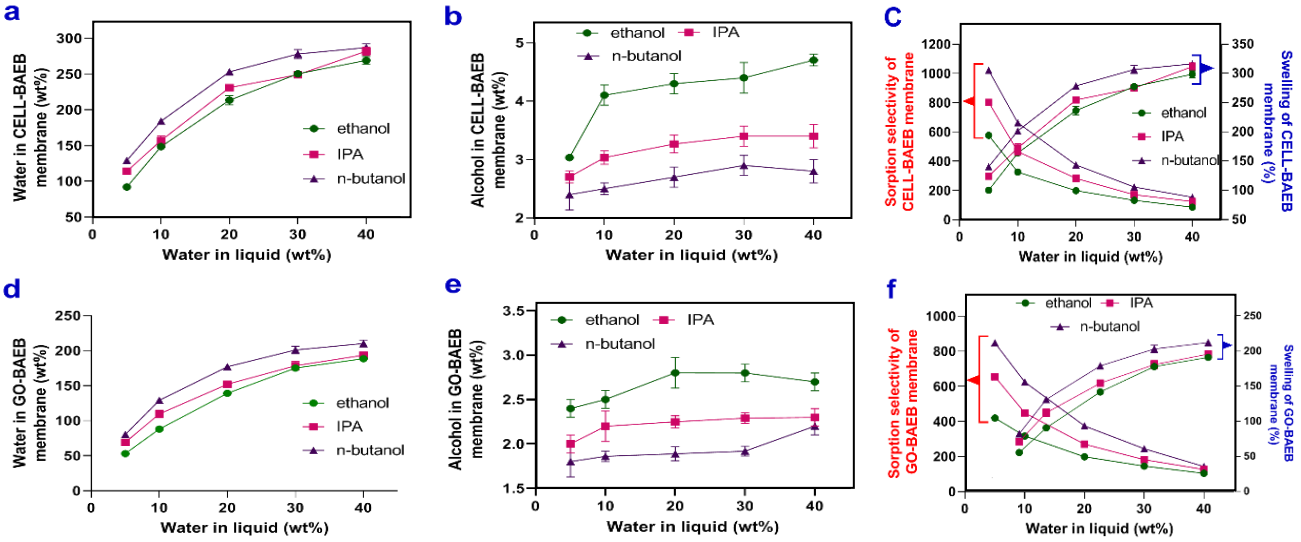

Fig. 6: The sorption behavior of CELL-BAEB and GO-BAEB in alcohols-water mixture vs. water content in solution; a and d) absorbed water (wt%) for CELL-BAEB and GO-BAEB membranes, b and e) absorbed alcohols (wt%) by CELL-BAEB and GO-BAEB membranes and c and f) swelling (wt%) and sorption selectivity of CELL-BAEB and GO-BAEB membranes.

which can be attributed to their higher hydrophilicity. DAC-BAEB has more grafted BAEB than GO-BAEB, and consequently, has higher hydrophilicity than GO-BAEB. Additionally, cellulose tends to absorb more water than GO due to its higher O-H groups, causing it to more swell in an alcohol-water solution [6]. The swelling of the IPA-water and n-butanol-water mixtures (Fig. 6c and Fig. 6f), also show a similar trend to those of the ethanol-water mixture, except that the slope of the water sorption and swelling graphs for the ethanol-water is greater than the slopes for the IPA-water and n-butanol-water solutions. The slope of the water in the membrane and the swelling graphs increase as ethanol-water < IPA-water < n-butanol-water. Polyionic materials do not only have an affinity to absorb water molecules but also exhibit repulsion to organic solvents through dipole-dipole interactions. Accordingly, with an increasing number of carbon atoms in alcohols, water sorption and swelling increase [60]. For CELL-BAEB, the water content was as high as 269 wt%, 276 wt%, 287 wt%, and for GO-BAEB, it was as high as 188 wt%, 193 wt%, and 211 wt% with 40 wt% water in the feed for ethanol, IPA, and n-butanol, respectively (Fig. 6a and Fig. 6d). The results show that these types of membranes have a high adsorption capacity and a high water selectivity.

Pervaporation measurements

An evaluation of a membrane's efficiency in separating solvents should be conducted in order to determine its pervaporation performance. Three parameters including 1) flux (Eq. (3), (2) water in permeate, and 3) separation factor (Eq. (4)) are widely used in pervaporation evaluation [61]. Fig. 7c and Fig. 7f illustrate the effect of feed temperature on the pervaporation performance of CELL-BAEB and GO-BAEB membranes (temperature range 40 to 70 ºC) in the dehydration of 10% ethanol, IPA, and n-butanol. Both membranes exhibit an increased permeation flux with increased feed temperatures, which is attributed to increased driving forces of water molecules into hydrophilic membranes. Over the entire temperature range, the water content in permeate is almost constant. This high-temperature stability can be assigned to the highly ionic cross-linking structure. CELL-BAEB and GO-BAEB membranes exhibit a progressive increase in total flux when the feed temperature increases while the water content in the permeate remains above 99 wt%. Using this characteristic, the total flux can be improved without compromising selectivity even at higher operating temperatures. The effect of feed composition with a water concentration of 5% to 40% was investigated at 70 °C on the separation performance of the CELL-BAEB and GO-BAEB membranes. As shown in Fig. 7, the total flux and water in permeate for CELL-BAEB and GO-BAEB membranes increased with the increasing percentage of water in feed, however, the total flux of CELL-BAEB was larger than that of GO-BAEB.

In both membranes, the total flux and the amount of water in the permeate increase due to an increase in the driving

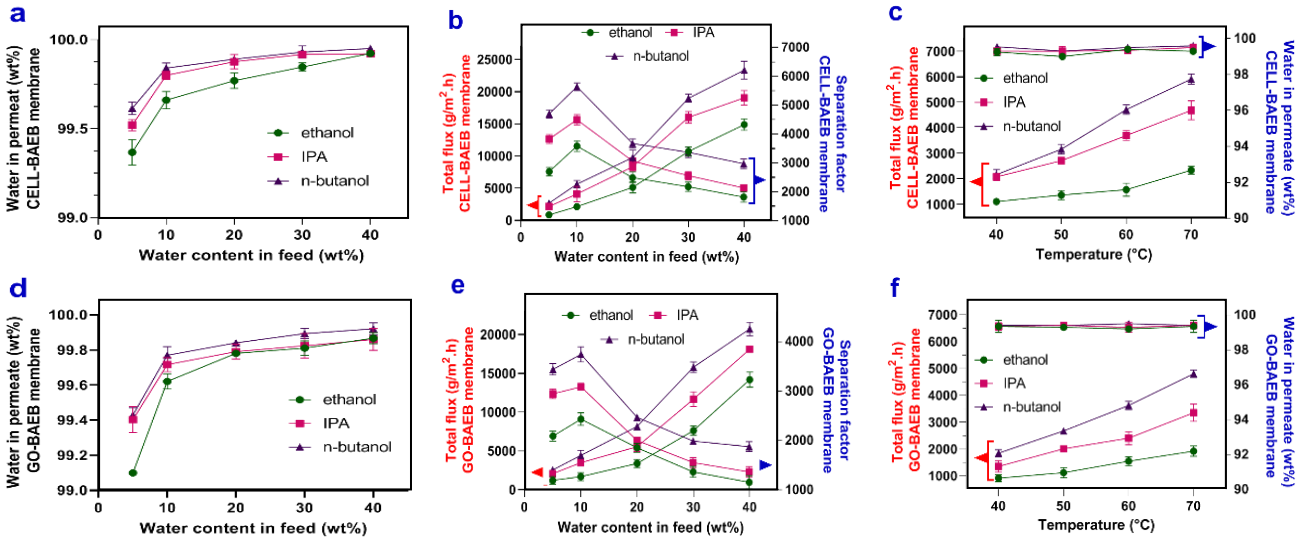

Fig. 7: Effect of feed composition (wt%) on a, d) water content in permeate (wt%), b, e) separation factor, and total flux (g/m^2.h) for CELL-BAEB and GO-BAEB membranes, and c, f) effect of feed temperature (^{o}C) on total flux (g/m^2.h) and water in permeate (wt%) for CELL-BAEB and GO-BAEB membranes. in dehydration of 10 wt% of ethanol, IPA and n-butanol in the temperature range 40 to 70 ^{o}C.

force of water into the membranes. The CELL-BAEB and GO-BAEB membranes exhibit a high attraction to water, resulting in extensive swelling [62]. Water absorption by CELL-BAEB and GO-BAEB membranes may cause them to swell to such a degree that some alcohol molecules are transferred into the membranes, resulting in decreased selectivity [63]. However, even at 5 wt% feed water content at 70 °C, the permeate water content remains above 99 wt%, showing that the cross-linked membranes are chemically stable and highly selective. Because the membranes are much hydrophilic, the separation factor also increases, and as expected, CELL-BAEB has a higher separation factor than GO-BAEB since there are more cross-linker molecules and water is more easily able to enter cellulose chains than GO sheets. The cross-linking with highly ionic molecules may change, not only their hydrophilicity but also their density, resulting in a decrease in the absolute free volume for the diffusion of permeate across the membranes. Thus, water molecules with relatively small molecular sizes may diffuse across membranes more easily than larger molecules of alcohol. Therefore, following expectation, the separation factor increases with increasing order of ethanol<IPA<n-butanol (Fig. 7b and Fig. 7e) [60]. Table 3 lists the pervaporation performance of some GO and cellulose-based membranes for dehydration of ethanol, IPA, and n-butanol. As compared to other membranes, the CELL-BAEB and GO-BAEB showed high performance for the dehydration of ethanol, IPA, and n-butanol.

CONCLUSIONS

In this research, CELL-BAEB and GO-BAEB membranes with highly ionic BAEB cross-linkers were synthesized and were shown as an efficient water-alcohol separation. The GO-BAEB and CELL-BAEB membranes exhibit high selectivity and permeability in the dehydration of ethanol, IPA, and n-butanol, a unique characteristic of these highly ionic membranes. The CELL-BAEB and GO-BAEB membranes showed excellent sorption and pervaporation performance in dehydration of 5-40 wt% water-alcohol mixtures. For example, the water content in the membrane was as high as 269 wt%, 276 wt%, 287 wt% for CELL-BAEB, and 188 wt%, 193 wt%, and 211 wt% for GO-BAEB in 40 wt% feed water at room temperature, and the separation factor was 3951, 4491, and 5616 for CELL-BAEB, and 2423, 3094, and 3741 for GO-BAEB, in 10 wt% feed water at 70 ^{o}C for ethanol, IPA, and n-butanol, respectively. Water content in the permeate was maintained above 99% in various feed water contents, indicating the high hydrophilicity of these membranes. This study provides a new strategy for designing dehydration membranes with optimized performances by the introduction of a highly hydrophilic cross-linking molecule into insoluble membrane matrixes.

Table 3: Alcohol dehydration performance comparison of GO-BAEB and CELL-BAEB membranes with some cellulose and GO-based membranes.

Membrane type	Binary mixture	Temperature (°C)	Separation factor	Total flux (g/m^2.h)	References
Current work, CELL-BAEB	Ethanol/H2O (90:10)	70	3951	2453	-
Current work, CELL-BAEB	IPA/H2O (90:10)	70	4491	4950	-
Current work, CELL-BAEB	n-butanol/H2O (90:10)	70	5616	6050	-
Current work, GO-BAEB	Ethanol/H2O (90:10)	70	2423	2055	-
Current work, GO-BAEB	IPA/H2O (90:10)	70	3094	3576	-
Current work, GO-BAEB	n-butanol/H2O (90:10)	70	3741	4906	-
Chitosan/poly (sodium vinyl-sulfonate)	Ethanol/H2O (90:10)	70	2700	1980	[64]
Chitosan cross-linked with sulfate	IPA/H2O (85:15)	80	200	1600	[65]
QP4VP/CMCNa	n-butanol/H2O (90:10)	60	1100	2241	[60]
Sodium alginate coated PEGylated GO	Ethanol/H2O (90:10)	70	660	2500	[66]
GO/ceramic	IPA/H2O (90:10)	70	2700	1800	[67]
GO/mPAN	n-butanol/H2O (90:10)	60	1791	4340	[68]

Acknowledgments

We gratefully acknowledge the financial support of Lorestan University.

Received: Dec. 31, 2023; Accepted: May. 29, 2023

REFERENCES

[1] Mouhat F., Coudert F.X., Bocquet M.L., Structure and Chemistry of Graphene Oxide in Liquid Water from First Principles, *Nat. Commun.*, **11:** 1566 (2020).

[2] Li T.C., Chen A.H., Brozena J.Y., Zhu L., Xu C., Driemeier J., Dai O.J., Rojas A., Isogai L., Wågberg L., Developing Fibrillated Cellulose as a Sustainable Technological Material, *Nature*, **590:** 47-56 (2021).

[3] Liang S., Song Y., Zhang Z., Mu B., Li R., Li Y., Yang H., Wang M., Pan F., Jiang Z., Construction of Graphene Oxide Membrane through Non-Covalent Cross-Linking by Sulfonated Cyclodextrin for Ultra-Permeable Butanol Dehydration, *J. Membr. Sci.*, **621:** 118938 (2021).

[4] Li L., Lu Y., Li L., Yang J., Fu W., Luo Y., Lu J., Zhang Y., Zhou L., Highly Selective Zeolite T Membranes with Different ERI Stacking Faults for Pervaporative Dehydration of Ethanol, *J. Membr. Sci*., **638:** 119701 (2021).

[5] Ma J., Ping D., Dong X., Recent Developments of Graphene Oxide-based Membranes: A Review, *Membranes*, **7(3):** 52 (2017).

[6] Shao L. Lia Y., Pana F., Zhang Z., Liang S., Wang Y., Zou J., Jiang Z., Graphene Oxide Membranes Tuned by Metal-Phytic Acid Coordination Complex for Butanol Dehydration, *J. Membr. Sci*., **638:** 119736 (2021).

[7] Esmaeili-Faraj S.H., Hassanzadeh A., ShakeriankhooF., Hosseini S., Vaferi B., Diesel Fuel Desulfurization by Alumina/Polymer Nanocomposite Membrane: Experimental Analysis and Modeling by the Response Surface Methodology, *Chem. Eng. Process.: Process Intensif*., **164:** 108396 (2021).

[8] Corra S., Curcio M., Baroncini M., Silvi S., Credi A., Photoactivated Artificial Molecular Machines that Can Perform Tasks, *Adv. Mater*., **32(20):** 1906064 (2020).

[9] Jyothia M.S., Reddy K.R., Soontarapa K., Naveenc S., Raghuc A.V., Kulkarnid R.V., Suhase D.P., Shettif N.P., Nadagoudag M.N., Aminabhavih T.M., Membranes for Dehydration of Alcohols *via* Pervaporation, *J. Membr. Sci*., **242:** 415-429 (2019).

[10] Khalid A., Aslam M., Abdul Qyyum M., Faisal A., Laeeq Khan Asim., Ahmed F., Lee M., Kim J., Jang N., Chang I.S, Bazmi A.A., Yasin M., Membrane Separation Processes for Dehydration of Bioethanol from Fermentation Broths: Recent Developments, Challenges, and Prospects, *Renewable Sustainable Energy Rev*., **105**:427-443 (2019).

[11] Wu Y., Ding L., Lu Z., Deng J., Wei Y., Two-Dimensional MXene Membrane for Ethanol Dehydration, *J. Membr. Sci*., **590:** 117300 (2019).

[12] Walther T., Francois J.M., Microbial Production of Propanol, *Biotechnol. Adv*., **34(5):** 984-996 (2016).

[13] Shi G.M., Chung T.S., Thin Film Composite Membranes on Ceramic for Pervaporation Dehydration of Isopropanol, *J. Mem. Sci*., **448:** 34-43 (2013).

[14] Harvey B.G., Meylemans H.A., The Role of Butanol in the Development of Sustainable Fuel Technologies, *J. Chem. Tech. Biotech*., **86:** 2-9 (2011).

[15] Castro-Muñoz R., Galiano F., Fíla V., Drioli E., Figoli A., Mixed Matrix Membranes (MMMs) for Ethanol Purification through Pervaporation: Current State of the Art, *Rev. Chem. Eng*., **35(5):** 0115 (2018).

[16] Hosseini M., "Advanced Bioprocessing for Alternative Fuels, Biobased Chemicals, and Bioproducts", Woodhead Publishing, The University of Texas, United States (2019).

[17] Venkata Mohan S., Varjani S., Pandey A., "Microbial Electrochemical Technology", Elsevier Publication (2019).

[18] Marjani A., Mechanistic Modeling of Organic Compounds Separation from Water via Polymeric Membranes, *Iran. J. Chem. Chem. Eng. (IJCCE)*, **36(6):** 139-149 (2017).

[19] Torkaman R., Kazemian H., Soltanieh M., Removal of BTX Compounds from Wastewaters Using Template Free MFI Zeolitic Membrane, *Iran. J. Chem. Chem. Eng. (IJCCE)*, **29(4):** 91-98 (2011).

[20] Liu G., Jin W., Pervaporation Membrane Materials: Recent Trends and Perspectives, *J. Membr. Sci*., **636:** 119557 (2021).

[21] Haresh K.D., Kaushik N., Acetic Acid Separation as a Function of Temperature Using Commercial Pervaporation Membrane, *Iran. J. Chem. Chem. Eng. (IJCCE)*, **38(3):** 283-292 (2019).

[22] Liu P., Chen M., Ma Y., Hu C., Zhang Q., Zhu A., Liu Q., A Hydrophobic Pervaporation Membrane with Hierarchical Microporosity for High-Efficient Dehydration of Alcohols, *Chem. Eng. Sci*., **206:** 489-498 (2019).

[23] Rahimalimamaghani A., Pacheco Tanaka D.A., Liosa Tanco M.A., Neira D'Angelo F., Gallucci F., New Hydrophilic Carbon Molecular Sieve Membranes for Bioethanol Dehydration via Pervaporation, *J. Chem. Eng*., 435: 134891 (2022).

[24] Bolto B., Hoang M., Xie Z., A Review of Membrane Selection for the Dehydration of Aqueous Ethanol by Pervaporation, *Chem. Eng. Proc*., **50:** 227-235 (2011).

[25] Amnuaypanich S., Kongchana N., Natural Rubber/Poly(Acrylic Acid) Semi-Interpenetrating Polymer Network Membranes for the Pervaporation Water–Ethanol Mixtures, *J. Appl. Polym. Sci*., **114:** 3501-3509 (2009).

[26] Li J., Zhang L., Gu J. Sunb Y. Ji X., Cross-Linking of Poly (Vinyl Alcohol) with N, N′-Methylene Bisacrylamide via a Radical Reaction to Prepare Pervaporation Membranes, *RSC Adv*., **5:** 19859-19864 (2015).

[27] Amirilargani M., Sadatnia B., Poly (Vinyl Alcohol)/Zeolitic Imidazolate Frameworks (ZIF-8) Mixed Matrix Membranes for Pervaporation Dehydration of Isopropanol, *J. Membr. Sci*., **469:** 1-10 (2014).

[28] Xu S., Wang Y., Novel Thermally Cross-Linked Polyimide Membranes for Ethanol Dehydration via Pervaporation, *J. Membr. Sci*., **496:** 142-155 (2015).

[29] Huang Y.H., Huang S.H., Chao W.C., Li C.L., Hsieh Y.Y., Hung W.S., Liaw D.J., Hu C.C., Lee K.R., Lai J.Y., A Study on the Characteristics and Pervaporation Performance of Polyamide Thin-Film Composite Membranes with Modified Polyacrylonitrile as Substrate for Bioethanol Dehydration, *Polym. Int.*, **63:** 1478-1486 (2014).

[30] Dmitrenko M., Kuzminova A., Zolotarev A., Ermakov S., Roizard D., Penkova A., Enhanced Pervaporation Properties of PVA-based Membranes Modified with Polyelectrolytes. Application to IPA Dehydration, *Polymers*, **12(1):** 14 (2020).

[31] Liu G., Wei W., Jin W., Pervaporation Membranes for Biobutanol Production, *ACS Sustainable Chem. Eng*., **2:** 546−560 (2014).

[32] Shah K.W., Wang S.X., Soo S.X.Y., Xu J., Viologen-based Electrochromic Materials: from Small Molecules, Polymers and Composites to Their Applications, *Polymers*, **11(11):** 1839 (2019).

[33] An Q., Huanga T., Shi F., Covalent Layer-by-Layer Films: Chemistry, Design, and Multidisciplinary Applications, *Chem. Soc. Rev*., **47:** 5061-5098 (2018).

[34] Heydari M., Moheb A., Ghiaci M., Masoomi M., Effect of Cross-Linking Time on the Thermal and Mechanical Properties and Pervaporation Performance of Poly(Vinyl Alcohol) Membrane Cross-Linked with Fumaric Acid Used for Dehydration of Isopropanol, *Appl. Polym. Sci*., **128(3):** 1640-1651 (2013).

[35] Xu S., Wang Y., Novel Thermally Cross-Linked Polyimide Membranes for Ethanol Dehydration *via* Pervaporation, *J. Membr. Sci*., **496:** 142-155 (2015).

[36] Liang S., Song Y., Zhang Z., Mu B., Li R., Li Y., Yang H., Wang M., Pan F., Jiang Z., Construction of Graphene Oxide Membrane through Non-Covalent Cross-Linking by Sulfonated Cyclodextrin for Ultra-Permeable Butanol Dehydration, *J. Membr. Sci*., **621:** 118938 (2021).

[37] Hung W.S., Tsou C.H., Guzman M.D., An Q.F., Liu Y.L., Zhang Y.M., Hu C.C., Lee K.R., Lai J.Y., Cross-Linking with Diamine Monomers to Prepare Composite Graphene Oxide-Framework Membranes with Varying d-Spacing, *Chem. Mater*., **26(9):** 2983–2990 (2014).

[38] Ding W., Wu Y., Sustainable Dialdehyde Polysaccharides as Versatile Building Blocks for Fabricating Functional Materials: An Overview, *Carbohydr. Polym*., **248:** 116801 (2020).

[39] Zhang L., Yan P., Lia Y., He X., Dai Y., Tan Z., Preparation and Antibacterial Activity of a Cellulose-based Schiff base Derived from Dialdehyde Cellulose and L-Lysine, *Ind. Crops. Prod*., **145:** 112126 (2020).

[40] Vrettos K., Karouta N., Loginos P., Donthula S., Gournis D., Georgakilas V., The Role of Diamines in the Formation of Graphene Aerogels, *Front. Mater*., **5:** 20 (2018).

[41] Stadermann M., Baxamusa S.H., Ruddle C.A., Chea M., Li S., Youngblood K., Suratwala T., Fabrication of Large-Area Free-Standing Ultrathin Polymer Films, *J. Vis. Exp*., **100:** 52832 (2015).

[42] Xu Y., Yu S., Peng G., Sotto A., Ruan H., Shen J., Gao C., Novel Crosslinked Brominated Polyphenylene Oxide Composite Nanofiltration Membranes with Organic Solvent Permeability and Swelling Property, *J. Membr. Sci*., **620(15):** 118784 (2021).

[43] Leo R., Lecaros G., Ho S.Y., Tsai H.A., Hung W.S., Hu C.C., Huang S.H., Lee K.R., Lai J.Y., Ionically Cross-Linked Sodium Alginate and Polyamidoamine Dendrimers for Ethanol/Water Separation through Pervaporation, *Sep. Pur. Technol*., **275:** 119125 (2021).

[44] Ju H., Duan J., Lu H., Xu W., Cross-Linking with Diamine Monomers to Prepare Composite, A Single Rapid Route for the Synthesis of Reduced Graphene Oxide with Antibacterial Activities, *Chem. Mater*., **26:** 2983-2990 (2014).

[45] Paredes J.I., Rodi S.V., Alonso A.M., Tascón J.M.D., Graphene Oxide Dispersions in Organic Solvents, *Langmuir*, **24:** 10560-10564 (2008).

[46] Liu X., Neoh K.G., Kang E.T., Viologen-Functionalized Conductive Surfaces: Physicochemical and Electrochemical Characteristics, and Stability, *Langmuir*, **18(23):** 9041-9047 (2002).

[47] Yang D., Velamakanni A., Bozoklu G., Park S., Stoller M., Piner R.D., Stankovich S., Jung I., Field D.A., Ventrice C.A., Ruoff R.S., Chemical Analysis of Graphene Oxide Films after Heat and Chemical Treatments by X-Ray Photoelectron and Micro-Raman Spectroscopy, *Carbon*, **47:** 145-152 (2009).

[48] Song Y., Gao Y., Rong H., Wen H., Sha Y., Zhang H., Liu H.J., Liu Q., Functionalization of Graphene Oxide with Naphthalenediimide Diamine for High-Performance Cathode Materials of Lithium-Ion Batteries, *Sustain. Energy Fuels*, **2:** 803-810 (2018).

[49] Movagharnezhad N., Moghadam P.N., In Vitro Evaluation of Biopolymer Networks Based on Crosslinked Cellulose with Various Diamines, *J. Appl. Polym. Sci*., **132(41):** 5 (2015).

[50] Lindh J., Ruan C., Strømme M., Mihranyan A., Preparation of Porous Cellulose Beads *via* Introduction of Diamine Spacers, *Langmuir*, **32(22):** 5600-5607 (2016).

[51] Hu H., Zhao Z., Wan W., Gogotsi Y., Qiu J., Ultralight and Highly Compressible Graphene Aerogels, *Adv. Mater*., **25(15):** 2219-2223 (2013).

[52] Compton O.C., Dikin D.A., Putz K.W., Brinson L.C., Nguyen S.B.T., Electrically Conductive ''Alkylated'' Graphene Paper via Chemical Reduction of Amine-Functionalized Graphene Oxide Paper, *Adv. Mater*., **22(8):** 892-896 (2010).

[53] Ishak W.H.W., Ahmad I., Ramli S., Amin M.C.I.M., Gamma Irradiation-Assisted Synthesis of Cellulose Nanocrystal-Reinforced Gelatin Hydrogels, *Nanomaterials*, **8(10):** 749 (2018).

[54] Zhang L., Yan P., Lia Y., He X., Dai Y., Tan Z., Preparation and Antibacterial Activity of a Cellulose-based Schiff base Derived from Dialdehyde Cellulose and L-Lysine, *Ind. Crops. Prod*., **145**:112126 (2020).

[55] Li J., Liu D., Li B., Wang J., Han, S., Liu L., Wei H., A Bio-Inspired Nacre-Like Layered Hybrid Structure of Calcium Carbonate under the Control Ofcarboxyl Graphene, *Cryst. Eng. Comm*., **17:** 520–525 (2015).

[56] Vrettos K., Karouta N., Loginos P., Donthula S., Gournis D., Georgakilas V., The Role of Diamines in the Formation of Graphene Aerogels, *Front. Mater*., **5:** 20 (2018).

[57] Siller M., Amer H., Bacher M., Roggenstein W., Rosenau T., Potthast A., Effects of Periodate Oxidation on Cellulose Polymorphs, *J. Cheminformatics*, **22:** 2245-2261 (2015).

[58] Lindh J., Ruan C., Strømme M., Mihranyan A., Preparation of Porous Cellulose Beads via Introduction of Diamine Spacers, *Lang.*, **32(22):** 5600-5607 (2016).

[59] Gimenes M.L., Liu L., Feng X., Sericin/Poly(Vinyl Alcohol) Blend Membranes for Pervaporation Separation of Ethanol/Water Mixtures, *J. Membr. Sci*., **295:** 71-79 (2007).

[60] Liu T., An Q.F., Zhao Q., Lee K.R., Zhu B.K., Qian J.W., Jie-Gao C., Preparation and Characterization of Polyelectrolyte Complex Membranes Bearing Alkyl Side Chains for the Pervaporation Dehydration of Alcohols, *J. Membr. Sci*., **429:** 181-189 (2013).

[61] Wang Y., Shung T., Bernard C., Neo W., Gruender M., Processing and Engineering of Pervaporation Dehydration of Ethylene Glycol via Dual-Layer Polybenzimidazole (PBI)/Polyetherimide (PEI) Membranes, *J. Membr. Sci*., **378:** 339-350 (2011).

[62] Xing R., Pan F., Zhao J., Cao K., Gao C., Yang S., Liu G., Wu H., Jiang Z., Enhancing the Permeation Selectivity of Sodium Alginate Membrane by Incorporating Attapulgite Nanorods for Ethanol Dehydration, *RSC Adv.*, **6:** 14381-14392 (2016).

[63] Ghobadi N., Mohammadi T., Kasiri N., Kazemimoghadam M., Modified Poly(Vinyl Alcohol)/Chitosan Blended Membranes for Isopropanol Dehydration via Pervaporation: Synthesis Optimization and Modeling by Response Surface Methodology, *J. Appl. Poly. Sci*., **134(11):** (2017).

[64] Zheng P.Y., Ye C.C., Wang X.S., Chen K.F., An Q.F., Lee K.R., Gao C.J., Poly(Sodium Vinylsulfonate)/Chitosan Membranes with Sulfonate Ionic Cross-Linking and Free Sulfate Groups: Preparation and Application in Alcohol Dehydration, *J. Membr. Sci*., **510:** 220-228 (2016).

[65] Galiano F., Falbo F., Figoli A., Methanol Separation from Liquid Mixtures via Pervaporation Using Membranes, "Methanol Science and Engineering", 361-380, USA, (2018).

[66] Zhao D., Zhao J., Ji Y., Liu G., Liu S., Jin W., Facilitated Water-Selective Permeation *via* PEGylation of Graphene Oxide Membrane, *J. Membr. Sci*., **567:** 311-320 (2018).

[67] Li G., Shi L., Zeng G., Zhang Y., Sun Y., Efficient Dehydration of the Organic Solvents through Graphene Oxide (GO)/Ceramic Composite Membranes, *RSC. Adv*., **4:** 52012-52015 (2014).

[68] Tsou C.H., An Q.F., Lo S.C., Guzman M.D., Hung W.S., Hu C.C., Lee K.R., Lai J.Y., Effect of Microstructure of Graphene Oxide Fabricated through Different Self-Assembly Techniques on 1-Butanol Dehydration, *J. Membr. Sci*., **477:** 93-100 (2015).